Phonons transmission via atomic impurity chains grafted on 2D lattice

F. Lekadir, B. Bourahla, and M. Boucherrab

Faculty of Sciences, Mouloud Mammeri University, BP17RP, 15000, *Tizi-Ouzou, Algeria.*

Received 11 December 2024; accepted 24 February 2025

An analytical and numerical formalism is developed to study the influence of the various positions of atomic chain impurities (of type B) on the scattering and transmission vibration spectra in a 2D plane structure (of type A). To achieve this, we have opted for the matching technique. Theoretical formalism provides a complete description of the lattice dynamics and elastic wave propagation through impurity sites. More particularly, it allows the determination of the dynamical properties and localized vibration states of the atomic chain deposited on the planar system. Numerical calculations are performed for three different positions of a B-atom chain on a 2D lattice: top, bridge and hollow. The results show that the phonons associated with the grafted chain are strongly depending on the scattering frequency, elastic force parameters and the position of the impurities. In the three considered configurations, the presence of the atomic chain gives rise to localized vibration effects. The observed fluctuations spectra are related to vibration resonances due to coherent coupling between traveling phonons and the localized vibration modes in the neighborhood of the impurity chain sites.

Keywords: 2D-impurity chains; vibration spectra; phonons transmission and reflection.

DOI: https://doi.org/10.31349/RevMexFis.72.030502

1. Introduction

The study of the lattice dynamics at surfaces and low-dimensional systems provides an important tool characterizing the physical properties of 2D lattices, which is complementary to investigations of structural and physicochemical properties [1, 2]. Moreover, important surface phenomena, such as adsorption, diffusion or growth, can be significantly influenced by the dynamics of surface atomic sites [3, 4]. Today, progress in science makes it possible to manipulate and place atoms in atypical configurations on substrates [5]. The first demonstration dates back to 1989, when Eigler *et al*. [7] were able to deposit 35 individual xenon atoms on the surface of a flat Nikel substrate, via a scanning tunneling microscope to spell out the three letters of the IBM company. This was the first time in the history of scientific research that researchers managed to precisely position atoms of another type on a flat surface. Since the beginning of the 1980s, interest in surface dynamical properties has been stimulated by the development of two spectroscopical methods for the detection of surface phonons: inelastic helium scattering (HAS) [8, 9] and inelastic scattering of electrons (EELS) [10, 11]. Both techniques have been extensively described in several review articles. The goal has been to establish experimental dispersion curves and to provide an accurate interpretation of elastic and mechanical properties [12]. In addition, significant progress in the theoretical predictability of surface phonons, perturbed mesoscopic structures and dynamical films has been achieved via several theoretical methods, such as the slab method, the Green function method and molecular dynamics. Theoretical models typically employ the model of nearest and next-nearest neighbors force constants in the harmonic approximation [13]. Although extensive, this study of surface phonons has been limited to ideal surfaces [14]. Recently, the lattice dynamics (vibrational properties) of surfaces and low-dimensional mesoscopic structures have attracted increasing experimental and theoretical interest because of their use as components in high-technology devices [15, 16]. This type of disordered surface involves random steps, terraces, and inhomogeneities on the surface, such as adsorbates and substitutional impurities, etc. The surface dynamics of such defects intriguingly show useful properties [17]. The surface inhomogeneities and configuration modify the vibrational properties of the system in two ways: first, they can give rise to new modes localized in their neighborhood, and second, they scatter the bulk and surface phonons [18]. Consequently, the observed resonances in the scattering spectrum for an atomic surface containing atomic defects are a signature of the localization effects in the neighborhood of the perturbed domains [20]. In the present work, we present a model calculation for phonon scattering and elastic wave transmission across B monatomic chain impurities deposited (grafted) on a 2D-planar lattice, at three different positions. Our objective is twofold in this work. On the one hand, we want to understand the effect of the mass of the impurity B sites as well as their interactions with the perfect waveguide (their environment). On the other hand, we wish to study the impact of the variation in the position of the chain sites on phonon transport. Three possibilities exist for placing the B chain sites on the 2D planar lattice. The first case corresponds to the top position (situation where each B atom of the chain is placed above an atom of the A lattice), the second case describes the bridge position (each B site is placed between two successive atoms of the A sites), and the third case corresponds to the situation where the B atom is placed in the center of the four atoms of the A planar sites (hollow position). The main motivation of our

simulation and numerical calculation work is to predict the evolution of the thermo-physical properties of solid materials at the atomic scale. Furthermore, the different geometric arrangements make it possible to guide experimenters to select functional atomic devices for possible applications as sensor elements in the electronic domain at very specific frequency intervals. To address the problems of lattice dynamics and vibrational properties of different types of atomic configurations in the presence of defects and/or symmetry breaking, our research group has used the matching method [21–25] for a long period of time. By using this technique,we can study localized phenomena as well elastic-wave diffusion and transport by different types of implanted nanostructures. The advantage of the method is that it allows us to treat both aspects using the same mathematical framework. The next section presents the studied system and describes the dynamics and vibration modes of the model system. In Sub 2.1, we begin by introducing the essential features of the formalism we have applied. More particularly, we describe the perfect planar waveguide vibration modes and their group velocities. Subsection 2.2 presents a theoretical outline of scattering in a domain containing the deposited chain of B atoms. Section 3 revolves around the numerical results of the vibration transport and phononic properties for the three types of positions of the deposited atomic chain on the planar atomic 2D lattice.

2. The model of an atomic chain and its evanescent modes

To formulate the problem of phonon transmission and reflection by a grafted atomic chain and to illustrate the applied matching method, we consider an isolated atomic chain of atom B deposited on a square 2D lattice of atom A. An analysis is carried out for three different positions of the B atoms on the A lattice, as indicated in Fig. 1. The three simulated positions are, (a) top, (b) bridge and (c) hollow. The x- and y-directions are taken in the plane of the surface, whereas the z-direction is normal to the planar lattice. For simplicity, we take the same distance a between all adjacent sites in the two Cartesian directions of the perfect A lattice. The lattice dynamics of each of the three configurations shown in Fig. 1, are simulated and studied while taking into account the nearest central force constants and nearest neighbors under the harmonic approximation.

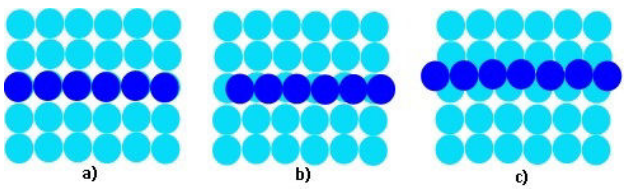

FIGURE 1. Schematic representation of a chain of impurity sites (B) grafted on a 2D structure (A), taking three different positions: a) top, b) bridge and c) hollow.

In the scattering region, which contains the impurity chain sites, the B atomic sites of the chain and their environment differ from the rest of the perfect 2D lattice in terms of their masses, which are m_A and m_B, respectively, and their elastic properties, where k_{1AA}, k_{1BB}, k_{1AB}, k_{2AA}, k_{2AB} stand, respectively, and the next and next-nearest strengths constant corresponding to interactions between atomic pairs A-A, A-B and B-B. To calculate the normalized frequencies in the system, we define the following different ratios for the planar waveguide and perturbed zone

$$\lambda = \frac{m_A}{m_B}, \quad r_1 = \frac{k_{1BB}}{k_{1AA}}, \quad r_1^{'} = \frac{k_{1AB}}{k_{1AA}},$$
$$r_2 = \frac{k_{2AA}}{k_{1AA}}, \quad r_2^{'} = \frac{k_{2AB}}{k_{1AA}}. \tag{1}$$

To carry out numerical simulations, we used the normalized interactions between different atomic sites of the considered model system. Our computer programs can operate for all possible values of the normalized interactions and the mass ration given in Eq. (1).

2.1. Dynamical properties of the perfect 2D lattice

The dynamics of the perfect planar 2D lattice can be described by the equations of motion of atomic sites l, which in harmonic the approximation [13] may be expressed as follows

$$m_l \omega^2 u_\alpha(l) = \sum_{l \neq l'} \sum_{\beta} k_{ll'} \frac{d_\alpha d_\beta}{d^2} \left\{ u_\beta(l') - u_\beta(l) \right\}. \tag{2}$$

Here, $m = ml$ is the atomic mass of the perfect 2D lattice located at site *l*, and *u* corresponds to its vibration displacement vector. Each atomic site can be identified by two indices $l = (i, j)$, where indices i and j count the sites along the x- and y-axes, respectively. The symbols α and β denote Cartesian coordinates. The radius vector d between two atomic sites located at l and l' has Cartesian components d_α, and $d = |d|$. The interactions between any two given sites are denoted by $k_{ll'}$, so that $k_{1ll'}$ and $k_{2ll'}$ are force constants between the nearest and next nearest neighbor sites, respectively. For two different atomic sites l and l' far from the inhomogeneous boundary of the deposited atomic chain illustrated in Fig. 1 (belonging to the perfect 2D lattice), the equations of motion may be cast in the following matrix form

$$\left[\Omega^2 I - M_p(r_2, Z, \exp(i\phi_y))\right] |u\rangle = |0\rangle, \tag{3}$$

the vector $|u\rangle$ denotes the vibration displacements along the main axes in a unit cell. The symbol I represents the identity matrix having the same rank as the dynamical matrix $M_p(2,2)$ of the perfect planar system. The vector $|u\rangle$ is a column vector containing all displacement of the unit cell of the perfect waveguide 2D lattice.

Along the main axes, we define the Bloch phase factors by $Z = \exp(i\phi_x)$ and $\exp(i\phi_y)$ between neighboring sites in the 2D-unit cell. Both notations ϕ_x and ϕ_y refer to dimensionless normalized wave vectors, defined as $\phi_x = q_x a$ and

$\phi_y = q_y a$, where the constant *a* defines the lattice spacing between all neighboring sites as well as over the perturbed region, neglecting any relaxation effects in the considered waveguides. The doublet (q_x, q_y) corresponds to the reciprocal components of the network wave vector. Therefore, the components (ϕ_x, ϕ_y) (equivalent to (q_x, q_y)) describe the angle of incidence of phonons in the studied 2D lattice. The last symbol $\Omega^2 = (\omega/\omega_0)^2$ constitutes the normalized frequency. Note that ω_0 is the characteristic frequency for the perfect planar waveguide. The Eq. (3) allows the diagonalization of the matrix M_p. The solutions - known as eigenvalues, yield the propagation phonon modes when $|Z| = 1$ and the evanescent vibration modes when $|Z| < 1$.

The exact solutions are obtained as a function of the normalized frequencies Ω and of the elastic force constants and elastic properties of the studied system. These solutions are obtained when the determinant vanishes, as presented in the equation below

$$det\left[\Omega^2 - M_p(r_2, Z, exp(i\phi_y))\right] = 0. \tag{4}$$

Notably, the complex phase factors are the solutions of Eq. (3), and we can obtain them via different procedures. In the present work, we used the one suggested by A. Khater *et al*. [26]. For the studied perfect planar lattice, the secular equation may consequently be expressed in polynomial form

$$\sum_{s=0}^{2} C_s Z^s = 0, \tag{5}$$

the coefficients $Cs = Cs(\Omega, r_2, \phi_y)$ are functions of the frequency Ω, phase factors and elastic constants of the 2D perfect waveguide. Owing to the Hermitian nature of the dynamics, the phase factors (Z, Z^{-1}) in the doublet symmetrically verify the polynomial forms [27]. We mention that only one of the two modes, which are solutions to Eq. (5), is of physical interest. Importantly, in all cases of dynamical lattices, the propagating vibration modes are referred to by the factor Z, and their inverses (defined by Z^{-1}) constitute phonon modes propagating in the opposite sense. Furthermore, if the modes are nonpropagating, we consider only the evanescent

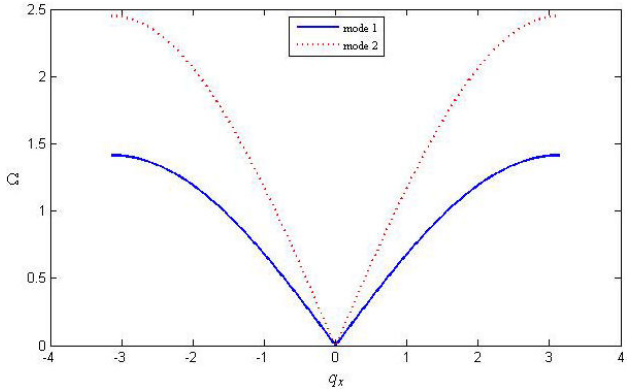

FIGURE 2. Typical phonon dispersion curves for the perfect planar waveguide, with a ratio of force constants $r_2 = k_2/k_1 = 0.5$, presented over the first Brillouin zone. The chosen value of r_2 can be encountered in certain real structures.

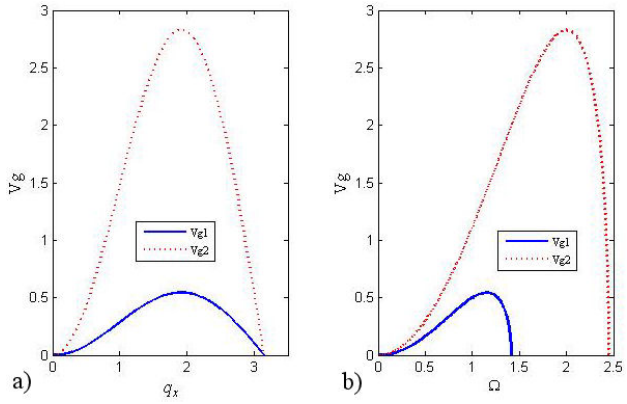

FIGURE 3. Curves of the normalized group velocities of the phonon propagation modes in the perfect planar structure, a) as a function of the wave-vector (on the left-hand side), b) as a function of the scattering frequency Ω (on the right-hand side).s

modes that satisfy the condition. Otherwise, the modes are divergent. To illustrate the elastic wave dispersion in the simulated planar 2D lattice as a function of the normalized wave vector $\phi_x = q_x$ times a, where q_x runs over the first Brillouin zone, the phonon branches are plotted in Fig. 2.

The propagation of an elastic wave in a material medium occurs with speed. The speed that accompanies the movement of the vibration wave in the atomic lattice is called the "group velocity of the wave packet". It corresponds to the speed with which energy or information is transported in a dispersive medium. If the wave-vector q_x takes real values, the velocity is defined by the following relation

$$V_g = \frac{\partial \Omega}{\partial q_x}, \tag{6}$$

If the wave vector q_x is different from a real number, we impose $Vg = 0$. The group velocities with which the waves move in the perfect 2D waveguide are shown in Fig. 3.

2.2. Impurity atomic chain dynamics

To analyze phonon transport and elastic wave diffusion via the chain of B atoms grafted onto a square lattice A, as shown in Figs. 1a)-1c), it is imperative to consider both the vibrational propagation modes and the evanescent modes in the systems studied via simulation. In another formulation, for a given frequency Ω and at a fixed incidence, we need all the solutions Z_n, including the solutions describing the propagating modes and those called evanescent, that is for $|Z_n| < 1$. The placement of the B impurity chain completely modifies the vibrational and mechanical properties of the 2D structure. The waves scattered by inhomogeneity depend on the amplitude and frequency of the incident elastic waves. Since the perfect waveguide does not couple all of the eigenmodes, we can treat the wave scattering problem for each mode separately. Consequently, we can redo the work for each phonon mode without any problem. Ultimately, the diffuse waves are

composed of reflected and transmitted waves, which generate a vibrational field on either side of the zone containing the chain of impurities, otherwise known as the "scattering region". In the A planar lattice, the evanescent and propagating vibration fields are effectively described by the phase factor doublets $[Z_n, Z_n^{-1}]$, which describe the solutions when going from one column to its nearest neighbors along the x-axis of the 2D perfect waveguide. When an elastic wave propagates from left to right via the scattering zone, in vibration eigenmode n, the α-components of the vibrational amplitude $u(i,j)$ for each atomic site located before the scattering zone, can be written, via the matching method, as a superposition of reflected and incident elastic waves [21, 25]. They are expressed as follows

$$u_\alpha(i,j) = Z_n^i u_n + \sum_1^2 R_{nn'} Z_{n'}^{-i} u_{n'}, \;\; i \leqslant l_1, \qquad (7)$$

for an atomic site after the scattering domain, the Cartesian α-components of the amplitude displacement $u\alpha^{'}(i,j)$, along the x-direction $i \in [l_1, l_2]$, can be expressed by an appropriate superposition of the vibration eigenmodes of the perfect waveguide transmitted at the frequency Ω, they are expressed as follows

$$u(i,j)_\alpha^{'}(i,j) = \sum_1^2 T_{nn'} Z_{n'}^{i} u_{n'}, \;\; i \geqslant l_2. \qquad (8)$$

To have access to all the solutions of Eqs. (7)-(8), we should first know the two quantities $T_{nn'}$ and $R_{nn'}$. Therefore, to achieve this objective, we consider a Hilbert space for the scattering process, and we have posed $[|u_R\rangle, |u_T\rangle]$ as the basis vectors of the reflection and transmission coefficients and $[|u_s>]$ as the basis vector of the irreducible atomic sites that contain the impurity B chain. Thus, the equations of motion of irreducible sites coupled to the borders of the two perfect sublattices located on both sides of the disturbed zone, should be expressed as a function of the vector $[|u_R\rangle, |u_T\rangle, |u_s\rangle]$. For the purpose of obtaining the matrix dynamics in the presence of the grafted chain in each position (as shown in Fig. 1), we should write the equations of motion of the irreducible sites as well as those of the two matching sites. The result is the obtaining of rectangular matrix forms M_d. The sizes of the dynamical matrices corresponding to each position of the impurity sites are given as follows: $M_d(16,20)$, for the top position shown in Fig. 1a); $M_d(13,17)$, for the bridge and hollow positions shown, respectively, in Fig. 1b)-1c). Importantly, the atomic sites in the scattering zone have a 3D configuration, and the movement along the z-axis is taken into account.

The matching method consists of expressing all the atomic displacements of the perturbed system as a function of the amplitudes of the irreducible sites and the boundary sites as well as the matching quantities. The latter comes from the study of the perfect 2D lattice and contains the characteristics of the incident wave. The obtained results can be grouped into a matrix M_R, called the matching matrix, whose elements are generated by relations (7)-(8). Consequently, the M_R size is the inverse of M_d. The matrix product $M_d \times M_R$ defines a square matrix (denoted M) and transforms the system to the linear one to allow its resolution. Specifically, for the studied positions, we obtain the square matrix dimensions M(16,16), for the structure of Fig. 1a); M(13,13), for the structures of Figs. 1b) and 1c). To solve the inhomogeneous linear system, we calculate

$$\left[\Omega^2 I - M(\lambda, r_1, r_1^{'}, r_2, r_2^{'}, \exp(i\phi_y))\right] \times [|u_s\rangle, |u_R\rangle, |u_T\rangle] = -|inh\rangle . \qquad (9)$$

where the vector $-|inh\rangle$ of the second member contains all the inhomogeneous terms describing the incoming elastic wave. The solution to Eq. (8) provides us with the atomic displacements of the irreducible sites located between the columns of the interval $[l_1, l_2]$, as well as the reflection and transmission coefficients $R_{nn'}$ and $T_{nn'}$ on the perfect 2D lattice. The diffusion phenomenon depends on the diffusion matrix, the elements of which are given by the relative reflection and transmission probabilities $r_{nn'}$ and $t_{nn'}$ at given Ω and ϕ_y, which are given by

$$r_{nn'}(\Omega, ph_y) = \frac{V_{gn}}{V_{gn}} |R_{nn'}|^2 ,$$
$$t_n(\Omega, ph_y) = \frac{V_{gn'}}{V_{gn}} |T_{nn'}|^2 . \qquad (10)$$

To guarantee the unitarity of the scattering matrix, the group velocities must normalize the scattered waves. Here, V_{gn} represents the group velocity of the eigenmodes. It is zero in the case of evanescent modes. We can define the total probabilities of reflection and transmission per given vibration mode at a scattering frequency Ω and a fixed direction ϕ_y by adding all the contributions

$$r_n(\Omega, ph_y) = \sum_{n'} r_{nn'}(\Omega, ph_y),$$
$$t_n(\Omega, ph_y) = \sum_{n'} t_{nn'}(\Omega, ph_y). \qquad (11)$$

To describe the overall transmission of the simulated systems, it is important to define the conductance (also called transmittance) of the grafted lattices by summing all the input and output modes

$$\sigma(\Omega, \phi_y) = \sum_n \sum_{n'} t_{nn'}(\Omega, \phi_y), \qquad (12)$$

the sum is made over the two propagation phonon modes at a given Ω and ϕ_y. However, it is worth mentioning that the conductance of a given system can be determined experimentally.

3. Numerical applications and discussions

The curves of the phonon dispersion in the simulated planar 2D lattice are presented in Fig. 2, as a function of the normalized wavevector ϕ_x over the first Brillouin zone. These curves can be plotted for any choice of the value of r_2. In addition, the usefulness of the value of the ratio r_2 lies in the fact that it allows us to illustrate our numerical model calculation systems with regard to vibrational properties. In the perfect waveguide, the choice of the fixed ratio: $r_2 = 0.5$ is arbitrary, not being dictated by any consideration, the interaction between next nearest neighbors $k_2 = 1/2$ of k_1 for the first nearest. Therefore, our calculation programs can run any value of r_2. Moreover, our simulations are conducted with normalized values. The advantage of the latter is that they allow computer programs to be executed without knowing the exact values of the force constants.

As shown in Fig. 2, the two eigenmodes 1,2 tend to propagate in the following frequency intervals: $\Omega_1 = [0.00; 1.41]$ and $\Omega_2 = [0.00; 2.45]$. Figure 2 shows that both modes are acoustical; they are characterized by limiting behavior Ω tending to zero when ϕ_x tends to zero. The mode numbering is also arbitrary, and we have opted for the length of the existence interval of each mode as a criterion. Furthermore, the branches related to the vibration modes have a nonlinear form but an arbitrary shape. This means that the structure is dispersive. Calculating the slopes of the tangents to the dispersion curves is a direct measure of group velocities. These are shown in Fig. 3.

In Fig. 3a), the group velocities are plotted as a function of the propagating frequency interval, whereas in Fig. 3b), the group velocities are presented as a function of the wavevector. We notice that the limits of each group velocity (nonzero) correspond well to the interval of excitation or the existence of the related phonon mode. Additionally, mode 2 (the most energetic mode) generates a large amplitude of group velocity, and the same information is confirmed in Fig. 3b). Therefore, a large involvement of mode 2 in phonon transport can be expected. Another important observation is that when the slopes of the tangents of the dispersion curves are negative, the elastic waves change the direction of propagation. In summary, the group velocities are essential to determine because they intervene in the scattering process, and this is the main objective of our work. To study elastic wave scattering by the grafted impurity chain at three different positions, we consider an incident wave that propagates along the x-axis (from left to right) of the perfect 2D waveguide shown in Fig. 1. The model systems considered are applied to study the evolution of vibrational properties as a function of the position of the sites of the atomic chain grafted above the planar structure (top, bridge and hollow). For each position, we numerically simulate the diffusion through the impurity atoms, and we determine the transmission and reflection coefficients of the elastic waves on the basis of Eqs. (9)-(10).

In the present work, we set a twofold objective:

(1) to determine the impact of the mass of impurities.

(2) to identify the effect of the variation in force constants on the dynamics of the system under study.

Firstly, to achieve our objective, numerical simulations are carried out for three possibilities of the mass m_B in relation to the mass m_A (variations of on the order of 1/10).

a) $\lambda < 1$, to describe a light mass, (we remember that $\lambda = m_A/m_B$).

b) $\lambda \approx 1$, to describe similar masses,

c) $\lambda > 1$, the heavy mass is reported.

Secondly, to describe the effect of variations in the nanostructured elastic constants on the lattice dynamics, in the numerical calculations, we assumed variations on the order of 1/10 compared with those of the perfect 2D waveguide. The choice of 1/10 is motivated by geometric considerations. In other words, the structure does not deform since it retains its crystalline architecture. Therefore, for each m_B possible position, we analyze the three possible situations of the interaction constants in the perturbed domain. These possibilities are as follows:

i) $r_1 < 1, r_1^{'} < 1, r_2^{'} < r_2$, (softening - case),

ii) $r_1 \approx 1, r_1^{'} \approx 1, r_2^{'} \approx r_2$ (homogeneous - case),

iii) $r_1 > 1, r_1^{'} > 1, r_2^{'} > r_2$ (hardening - case).

Notably, interactions between the atomic sites of the 2D lattice and the sites of the chain are described by the constant k_{AB}. We take them as the arithmetic means of A and B, whose interaction constants with the nearest neighbors are $(k_A + k_B)/2$, and this is also valid for the 1st and 2nd neighbors. Notably, to our knowledge, no experimental results are available for use in simulations. Those available are based on alloy concentrations and not for ideal structures. The obtained results for vibration transmission/reflection spectra are expressed as a function of the scattering frequency Ω. They are plotted in Figs. 4, 5 and 6, respectively, for Figs. 1a), 1b) and 1c).

To In the previous figures, we represented the transmission and reflection coefficients t_1, r_1, t_2, r_2 and their sum s_1, s_2, as a function of the scattering frequency in the two vibrational modes of the systems shown in Fig. 1. They are arranged in rows to describe the two phonon modes (from 1 to 2) and in columns to describe the three simulated cases of elastic environments (cases (i), (ii) and (iii)). The first observation that stands out is the existence of some common characteristics for Figs. 4, 5 and 6, and the presence of other characteristics specific to each configuration or position of the chain of impurities, in all considered cases. Among the general characteristics, for the three positions of the B chain, we note the following:

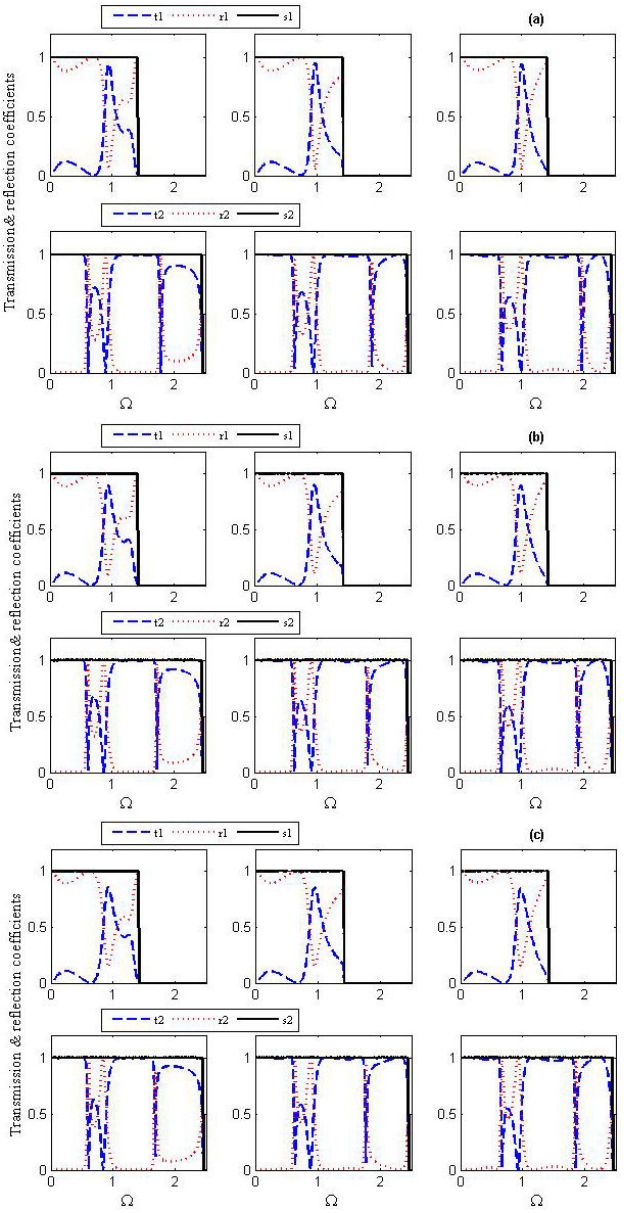

FIGURE 4. Curves of transmission t_1, t_2 (dotted lines) and reflection r_1, r_2 coefficients (dashed lines) and their sum s_1, s_2 (solid lines) for the first position of the impurity atoms on a planar structure of Fig. 1a), as a function of the scattering frequency Ω. The results are arranged in rows and columns. The former describes the two vibration modes and the latter refers to the simulated force coupling (from softening to hardening situations). a) The first case corresponds to a soft mass $(m_B < m_A)$. b) The second case corresponds to similar masses $(m_B = m_A)$. c) The third case corresponds to a heavy mass $(m_B > m_A)$.

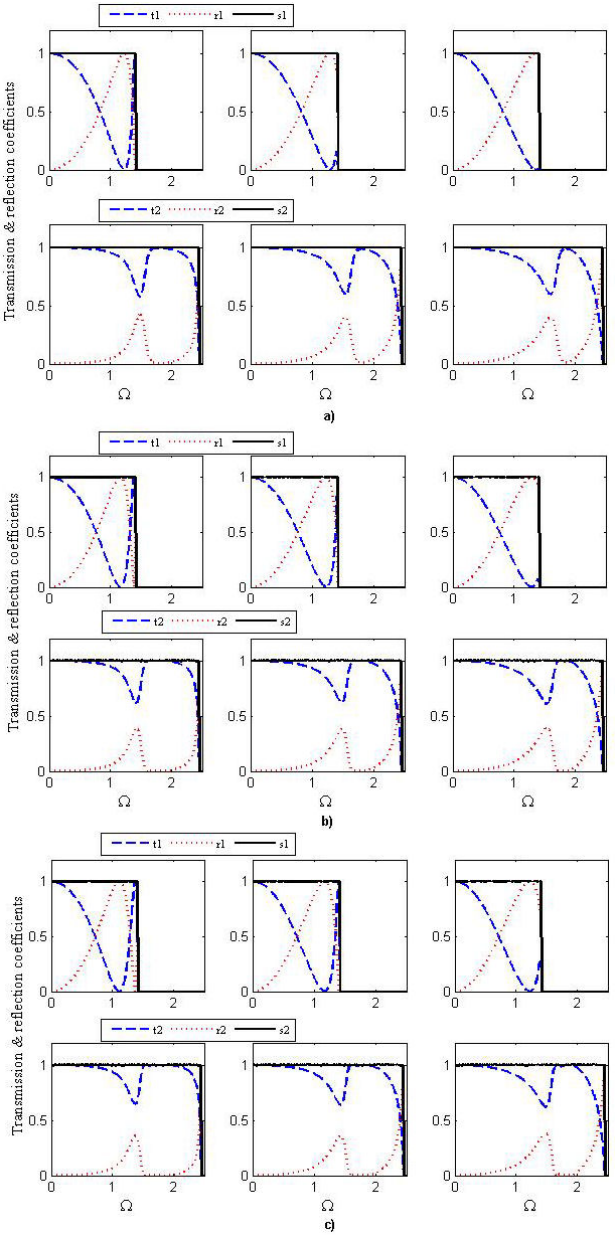

FIGURE 5. As in Fig. 4. The curves describe the vibration spectra relating to the impurity atoms grafted onto the 2D lattice, as schematized in Fig. b).

- Verification of the unitary condition, which reflects energy conservation, by the transmission and reflection coefficients $s = t_n + r_n = 1$, where $n = 1, 2$. This condition usually serves as a validation test of the numerical calculations, for the scattering matrices.
- All the transmission coefficients do not exceed the frequency interval where the group velocities are nonzero $(\Omega \leq 2.45)$.
- In the transmission and reflection spectra, there is a displacement of their spectral characteristics toward higher frequencies, hardening the force constants in the perturbed domain for the three configurations. This finding highlights the ability of the impurity chain sites to leave an intrinsic fingerprint on the transmission spectra of elastic waves. The configurations can be used to control (amplify or diminish) phonon transmission. The same behavior is observed with increasing the mass of the impurity sites, from soft to heavy (shifting of the spectra proportionally with increasing m_B).

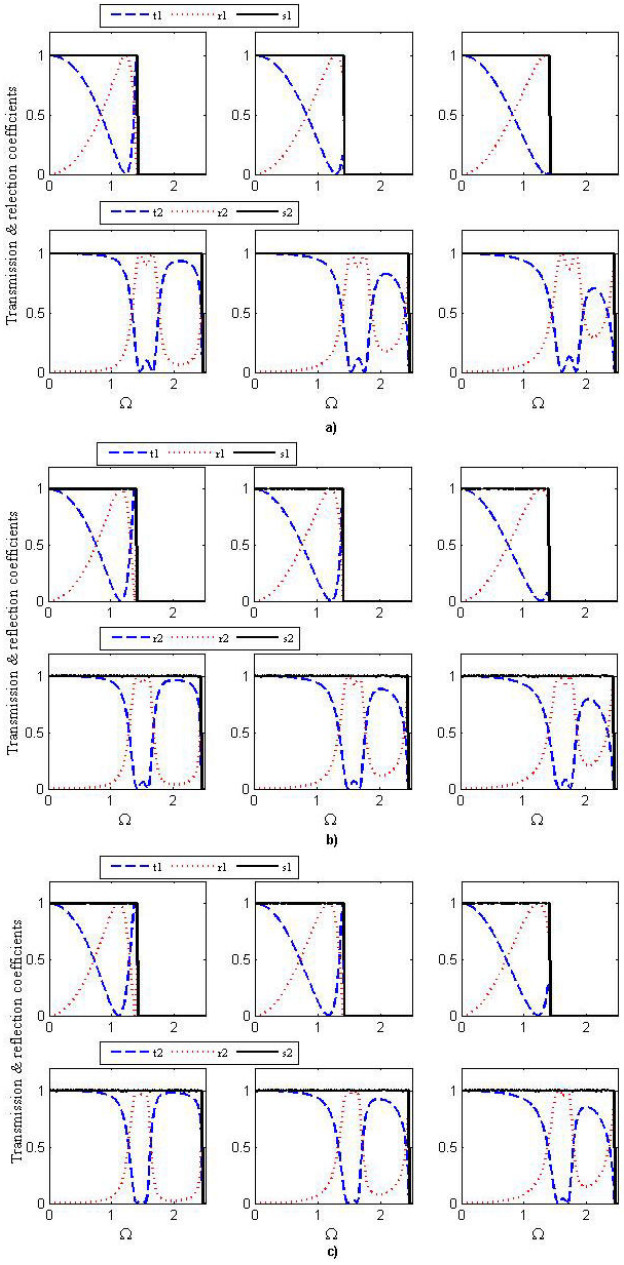

FIGURE 6. As in Fig. 4. The curves describe the vibration spectra relating to the impurity atoms grafted onto the 2D lattice, as schematized in Fig. 1c).

- All transmission coefficients t_1 and t_2 present fluctuations and vanish at the limit band frequencies. This is attributed to the coupling of the propagating incident phonons with a localized vibration mode induced by the atoms of the impurity chain. We also notice a specific behavior of the phonon, for each of the three configurations examined. More particularly, for the top position of the chain of B atoms Fig. 4, we observe that the transmission, according to mode 1, is very weak at low frequencies, whereas it is at its maximum in the case of vibration mode 2.

Since eigenmode 1 does not favor phonon transport, it is asymmetrically transverse in nature. The second eigenmode tells us about its acoustic and symmetrical nature because it gives rise to a vibration movement, which takes place horizontally with a wavelength very close to the lattice parameter. Additionally, in the transmission spectrum of each vibration mode, certain peaks are identified as Fano-type oscillations. More details on Fano resonances can be found in Refs. [28, 29]. This signals the existence of interactions in the scattering domain between the propagating phonon modes generated by the perfect 2D lattice and the localized states of the perturbed zone, which contains the grafted chain. Localized phonon states are dynamic vibrational states for which the amplitude of the atomic displacement decreases with distance from the perfect domain, which is consistent with the evanescent modes of the perfect 2D waveguide. The energies naturally shift to higher frequencies with increasing elastic constants in the perturbed domain. The other maxima fluctuations, in the spectra, correspond to the variation in the phonon transmission between the pinning minima that are imposed by the limits of the propagation intervals of the vibration modes. Furthermore, localized phonon states are dynamic vibrational states for which the amplitude of the atomic displacement decreases with distance from the perfect domain, being consistent with the evanescent modes of the 2D system. The energies naturally shift to higher frequencies with increasing elastic constants in the perturbed domain.

Figures 5 and 6 show that the transmission spectra evolve in a similar manner but not identical way. That is regardless of the position of the grafted chain (bridge or hollow), it has no impact on phonon transport at low energies in both vibration modes 1 and 2. As observed, the influence of the B atoms of the chain is nonexistent at low frequencies for t_1 and t_2 ; when Ω tends toward zero, they tend toward their maximum values (1). As we move up the frequency range, the coefficients are sensitive to the effect of the presence and position of the impurity chain. They behave differently at the frequency limit, depending on the ratio of the nearest and next-nearest neighbor constants. In both cases, t_1 and t_2 present spectra that are less rich in oscillations, with the system parameters. In addition, the behavior observed during the analysis of the results of the top position also remains valid for the other two positions. In other words, the transmission spectra generated by the two vibration modes shift proportionally toward the top of the definition interval with the hardening of the force constants as well as the increase in the mass of the impurity sites.

The comparison between Figs. 5 and 6 indicates the existence of a frequency range (at the center of the interval $(1.50 \leq \Omega \leq 1.80)$ where the transmission is very weak in the case of the hollow position. On the other hand, the bridge position only records a slight reduction in transmission. This result is remarkable: a simple variation in the position makes it possible to physically manufacture a phonon filter in a very specific frequency range. We can also identify the frequencies where phononic transport can be amplified. In the last

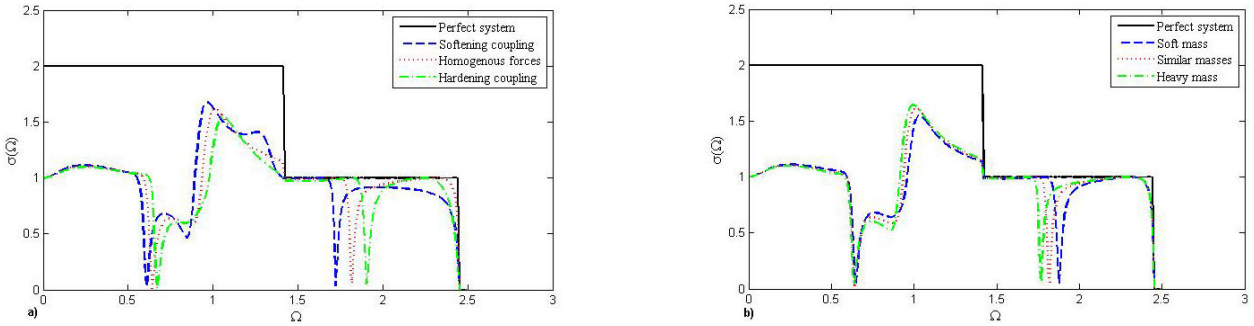

FIGURE 7. Curves of the vibration conductance spectra for the structure in Fig. 1a). They are determined in the propagating frequency interval of the perfect waveguide. a) We identify only the influence of force constants by simulating similar masses (m_B, m_A). b) We identify only the m B effect by considering the homogenous interactions case

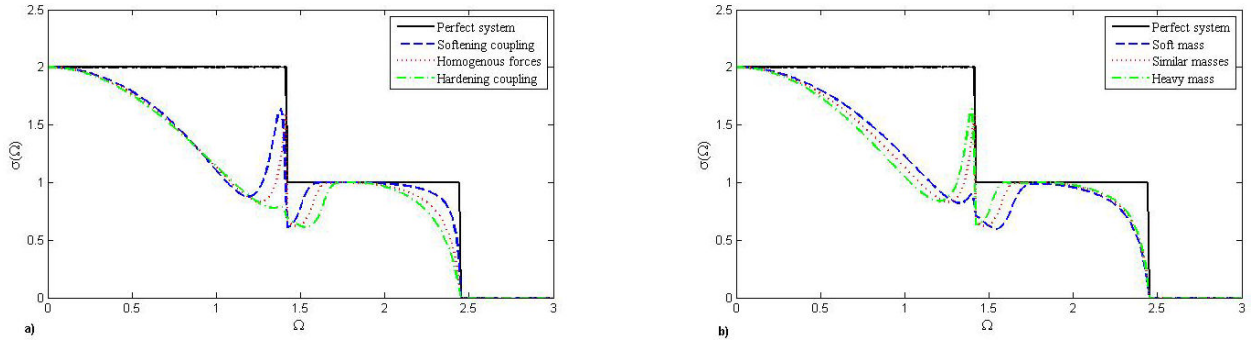

FIGURE 8. Like Fig. 7, it displays the phononic conductance of the structure shown in Fig. 1b).

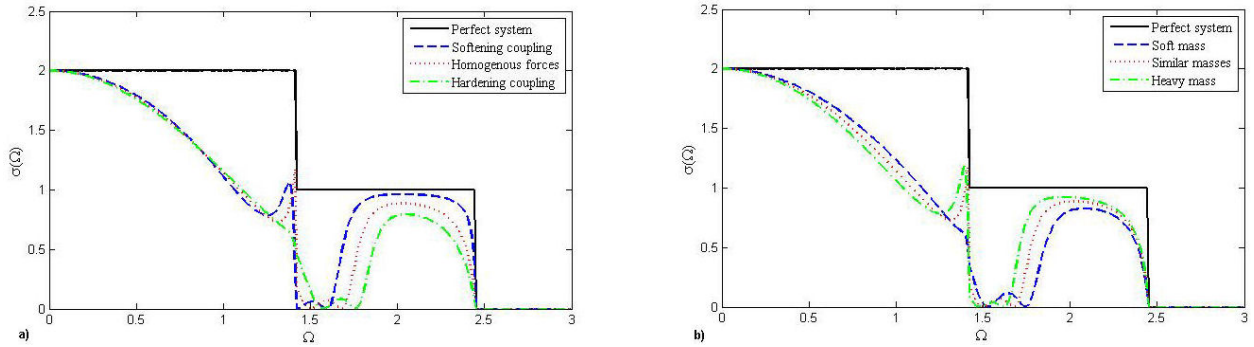

FIGURE 8. Like Fig. 7, it displays the phononic conductance of the structure shown in Fig. 1c).

part of the present work, we determined the phononic conductances (also called transmittances) through the B sites of the grafted impurity chain, which are placed at different positions. It is given by the application of Eq. (11). It represents the contribution of both modes (1 and 2) simultaneously to phononic transport.

To illustrate the calculations and to note separately the impact of the variation in mass (from soft to heavy) and the variation in interactions (from softening to hardening), we have opted for the representation of two cases among those presented in the present article. The results are shown in Figs. 7, 8 and 9, respectively, for the top, bridge and hollow positions. The curves are plotted as a function of the broadcast frequency Ω. The figures plotted are, respectively, for comparable masses (in (a)) and homogeneity of force constants (in (b)). Illustrate the calculations and to note separately the impact of the variation in mass (from soft to heavy) and the variation in interactions (from softening to hardening), we have opted for the representation of two cases among those presented in the present article. The results are shown in Figs. 7, 8 and 9, respectively, for the top, bridge and hollow positions. The curves are plotted as a function of the broadcast frequency Ω. The figures plotted are, respectively, for comparable masses (in (a)) and homogeneity of force constants (in (b)). Figure 7, the conductance starts with one (1). This means that one of the phonon eigenmodes has a particular behavior. It is transmitted weakly, or not at all; it is almost completely reflected in the propagation interval $\Omega \in [0, 1]$.

Technically, one may say that the top position filters phonons at low frequencies and that the vibration modes are decoupled.

The interval $\Omega \in [1, 1.41]$ constitutes the band where the transmittance is quite importnt for the top position. In addition, the structural conductance is less than or equal to one. On the other hand, in Figs. 8 and 9, the conductance spectrum always starts with its higher values at low frequencies (Ω tends to zero), fluctuates for intermediate values of Ω and decreases with increasing Ω; then it becomes zero at the Brillouin zone limit. For the studied configurations, we observe that the phonon conductance is less than or equal to one phonon throughout the propagating interval frequency ($\Omega \in [0, 2.45]$). This demonstrates the ability of the grafted atomic chain to restrict the phononic conductance in very specific frequency bands.

To be able to quantitatively determine the total transmission gap between the grafted chain (in each position) and the perfect structure (reference), we also traced the conductance of the perfect system. It is presented in the form of a histogram. The latter is made up of levels, where each level gives the number of vibration modes likely to be excited in the definition frequency interval. The number of modes relates well to the limits of the dispersion branches found in Fig. 2. An important feature of the phonon conductance is the shift of its spectral characteristics to higher frequencies with increasing hardening of the force constants in the perturbed domain, for the three different positions of the grafted chain (see the figures designated by the letter (a)). On the other hand, when the mass increases, the positions of the transmittance spectra shift toward lower frequencies (see the figures designated by the letter (b)). Therefore, increasing the B mass acts as a filter for the propagation of elastic waves.

With respect to the transmission spectra, some of the maximum fluctuations in the conductance spectra correspond to characteristic Fano resonances in the interval [0,2.45], since the atomic vibration states in the scattering zone are effectively localized states embedded in the perfect 2D waveguide incident phonon modes. In addition, the number of spectral fluctuations related to Fano resonances is in good agreement with localization theory. In light of what has been said thus far, one may claim that the conductance spectra can thus be considered fingerprints of the specific position of the grafted chain and therefore be used for characterization. The interaction between the states induced by impurities and the eigenmodes of the propagating waveguide could constitute an interesting alternative for studying the structural properties.

In all cases, the observed fluctuations in the vibration spectra are due to the increase in the number of localized vibration states around the grafted atomic chains. We remind that for greater experimental relevance, the models should incorporate finite size effects in the atomic lattices themselves.

4. Conclusions

The generic properties of elastic wave propagation in a monatomic 2D lattice (A) in the presence of a grafted atomic chain (B), placed at three different positions (top, bridge and hollow), are studied via the matching technique in the harmonic approximation. The results of the study show that the transmission vibration spectra and the phononic conductance of the system, with different positions of the grafted impurity B atoms, are functions of the scattering frequency, the impurity mass and the structure configuration. At lower frequencies, the conductance starts with its maximal values for the bridge and hollow configurations, fluctuates in the propagating interval frequency and becomes null at the Brillouin zone limit. For the top configuration, the impact of the B sites is considerably significant. The capacity of the perfect waveguide is reduced by half and then it reaches its maximum at the center of the interval. One may conclude that the geometry of the structure can filter certain elastic waves at low frequencies. The number of spectral fluctuations related to Fano resonances is in good agreement with localization theory. Each configuration type corresponds to a number of localized modes that interact with the propagating vibration modes of the perfect waveguide. Varying the parameters of the perturbed zones can modify the vibration properties (phonons transmission, localized vibration states, transmittance). This implies the possibility of a nanometric procedure to organize the heat transfer from a thermal or coherent source, preferentially, into different branches of a mesoscopic system. We mention that 2D structures, surfaces as well as semi-infinite systems constitute a fruitful area of research. The main reasons are that a variety of interesting effects can be artificially built into these types of materials. Additionally, a number of important applications rely on the ability to prepare functional atomic devices for well-defined uses. The incorporation of the structural inhomogeneities makes it possible to profoundly modify the physicochemical properties, in general, and the vibrational properties in particular. Knowledge of the dynamic matrix of the perturbed structures provides access to spectral densities as well as densities of states which have a direct impact on electronic transport and elastic waves scattering.

Aknowledgments

The author Fazia Lekadir expresses her gratitude to H. Hami for proofreading the manuscript.

1. G. Benedek *et al*., Measuring the electron-phonon interaction in two-dimensional superconductors with he-atom scattering, *Condensed Matter* **5** (2020) 79.
2. W. Z. Xiao, G. Xiao, and L. Wang, Two-dimensional hexagonal LaOF with ultrawide bandgap, large exciton energy, and low lattice thermal conductivity, *Physica E* **140** (2022) 115195.
3. H. Peng, and B. Zou, Effects of Electron-phonon coupling and spin-spin coupling on the photoluminescence of low-dimensional metal halides, *Journal of Physical Chemistry Letters* **13** (2022) 1752.
4. Q. Shen *et al*., Ultralow Thermal Conductivity and High Thermoelectric Performance Induced by Dimensionality Reduction in Chain-like Compounds X2PtSe2 (X= K, Rb), *Material Today Physics* **46** (2024) 101471.
5. D. Eigler, From the bottom up: building things with atoms, Nanotechnology, Springer, New York (1999) 425-435.
6. D. M. Eigler, and E. K. Schweizer, Positioning single atoms with a scanning tunnelling microscope, *Nature* **344** (1990) 524.
7. C. Toumey, 35 atoms that changed the nanoworld, *Nature Nanotechnology* **5** (2010) 239.
8. Y. W. Liu *et al*., An investigation of the anomalous asymptotic behavior of elastic electron scattering of helium, *The Journal of Chemistry Physics* **152** (2020) 034304.
9. C. J. Hatchwell, M. Bergin, B. Carr, M. G. Barr, A. Fahy, and P. C. Dastoor, Measuring scattering distributions in scanning helium microscopy, *Ultramicroscopy* **260** (2024) 113951.
10. K. Venkatraman, and M. Chi, Nanoscale Vibrational Spectroscopy in a Scanning Transmission Electron Microscope, *Encyclopedia of Nanomaterials* (2023) 251-261.
11. A. G. Nixon, M. Chalifour, M. R. Bourgeois, M. Sanchez, and D. J. Masiello, Inelastic scattering of transversely structured free electrons from nanophotonic targets: Theory and computation, *Physical Review A* **109** (2024) 043502.
12. C. Imediegwu, U. Grimm, R. Moat, and I. Jowers, A computational method for determining the linear elastic properties of 2D aperiodic lattice structures, *The Journal of Strain Analysis for Engineering Design* **58** (2023) 590.
13. P. Tangney, Wave theory of lattice dynamics, (2024), arXiv preprint arXiv:2401.02375.
14. B. Zheng *et al*., Ideal type-III nodal-ring phonons, *Phyical Review B* **101** (2020) 100303.
15. S. Xie, H. Zhu, X. Zhang, and H. Wang, A brief review on the recent development of phonon engineering and manipulation at nanoscales, *International Journal of Extreme Manufacturing* **6** (2023) 012007.
16. G. Chen, Phonon transport in low-dimensional structures, *Semiconductors and Semimetals* **71** (2001) 203.
17. O. E. Raichev, G. M. Gusev, F. G. G. M. Hernandez, A. D. Levin, and A. K. Bakarov, Phonon drag thermoelectric phenomena in mesoscopic two-dimensional conductors: Current stripes, large Nernst effect, and influence of electron-electron interaction, *Physical Review B* **102** (2020) 195301.
18. T. C. Phong, and N. D. Hien, Comparison of electron scattering by acoustic-phonons in two types of quantum wells with GaAs and GaN materials, *Nanoscale Advances* **6** (2024) 832.
19. A. Giri, B. F. Donovan, and P. E. Hopkins, Localization of vibrational modes leads to reduced thermal conductivity of amorphous heterostructures, *Physical Review Materials* **2** (2018) 056002.
20. A. Belayadi, B. Bourahla, and F. Mekideche-Chafa, Neurocomputing techniques to predict the 2D-structures by using lattice dynamics of surfaces, *Acta Physica Polonica A* **132** (2017) 1314.
21. J. Szeftel, F. Mila, and A. Khater, Structural investigation of the surface reconstructed system Ni(100)+(2-2)C using vibrational analysis, *Surface Science* **216** (1989) 125.
22. A. Belayadi, and B. Bourahla, Electronic quantum scattering across molecular junctions: Oligoacenes and oligophenyl graphene strips, *Computational Condensed Matter* **24** (2020) e00493.
23. B. Bourahla, and A. Belayadi, Computing the surface electronic states on the (100),(110) and (111) surfaces of fcc monatomic crystals, *International Journal of Modern Physics B* **35** (2021) 2150066.
24. S. Sait and B. Bourahla, Phonons transmission through atomic interface connecting two semi-infinite 2D lattices with different meshes, *International Journal of Modern Physics B* **36** (2022) 2250012.
25. R. Challali, S. Sait, B. Bourahla, and L. Ferrah, Localized Surface Magnon Modes in Cubic Ferromagnetic Lattices, *Spin* **13** (2023) 2350001.
26. A. Khater, and M. Belhadi, Phonon scattering via an atomic well in free standing thin solid films, *Surface Review Letters* **16** (2009) 271.
27. G. Belkacemi, and B. Bourahla, Heat transfer by metallic thin film sandwiched in semiconductor lattice, International *Journal of Modern Physics B* **31** (2017) 1750155.
28. N. Solodovchenko, M. Sidorenko, T. Seidov, I. Popov, E. Nenasheva, K. Samusev, and M. Limonov, Cascades of Fano resonances in light scattering by dielectric particles, *Materials Today* **60** (2022) 69.
29. Q. Zhao, C. Yao, Y. He, Y. Yang, and H. Zhang, Fano resonance and enhanced sensing in the excitation of the surface phonon polariton, *JOSA B* **41** (2024) 1099.